The Astrophysical Journal, 593:189–202, 2003 August 10

VLT+UVES SPECTROSCOPY OF THE Ca II LOW-IONIZATION BROAD ABSORPTION LINE QUASAR SDSS J030000.56+004828.0[1]

Patrick B. Hall,[2,3] Damien Hutsemékers,[4,5] Scott F. Anderson,[6] J. Brinkmann,[7] Xiaohui Fan,[8,9] Donald P. Schneider,[10] and Donald G. York[11,12]

Received 2003 January 28; accepted 2003 April 18

ABSTRACT

We study high-resolution spectra of the "overlapping-trough" low-ionization broad absorption line (LoBAL) quasar SDSS J030000.56+004828.0. The Ca II, Mg II, and Mg I column densities in this object are the largest reported to date for any BAL outflow. The broad Ca II absorption is mildly blended, but the blending can be disentangled to measure the Ca II column density, which is large enough that the outflow must include a strong hydrogen ionization front. The outflow begins at a blueshift of $\sim$1650 km s^{-1} from the systemic redshift. The lowest velocity BAL region produces strong Ca II absorption but does not produce significant excited Fe II absorption, while the higher velocity excited Fe II absorption region produces very little Ca II absorption. We have found that only a disk wind outflow can explain this segregation. Whether the outflow is smooth or clumpy, we conclude that the Ca II BAL region has a density high enough to populate excited levels of Fe II but a temperature low enough to prevent them from being significantly populated. This requirement means the Ca II BAL region has $T \lesssim 1100$ K, and perhaps even $T \lesssim 550$ K. This quasar also has an associated absorption line system (AAL) that exhibits partial covering and therefore is likely located near the central engine. Its association with the BAL outflow is unclear. Blending of the AAL with the BAL trough shows that the spatial region covered by the BAL outflow can vary over velocity differences of $\sim$1700 km s^{-1}.

Subject headings: quasars: absorption lines — quasars: emission lines — quasars: general — quasars: individual (SDSS J0300+0048)

On-line material: color figures

1. INTRODUCTION

One of the goals of the Sloan Digital Sky Survey (SDSS; York et al. 2000) is to obtain spectra for $\sim 10^5$ quasars to $i = 19.1$ ($i = 20.2$ for $z > 3$ candidates), in addition to the $\sim 10^6$ galaxies that comprise the bulk of the spectroscopic targets (Blanton et al. 2003). From astrometrically calibrated drift-scanned imaging data (Gunn et al. 1998; Pier et al. 2003) on the SDSS *ugriz* AB asinh magnitude system (Fukugita et al. 1996; Lupton, Gunn, & Szalay 1999; Hogg et al. 2001; Stoughton et al. 2002; Smith et al. 2002), quasar candidates are selected primarily through the use of color criteria designed to target objects whose broadband colors are different from those of normal stars and galaxies (Richards et al. 2002). Because of these inclusive criteria, the selection of candidates using *i*-band magnitudes rather than blue magnitudes (which are more affected by absorption and reddening), its area, and its depth, the SDSS is effective at finding unusual quasars (e.g., Fan et al. 1999). Many of these objects are unusual broad absorption line (BAL) quasars.

BAL quasars show absorption from gas with typical outflow velocities of $0.1c$ (Weymann et al. 1991) and mass-loss rates probably comparable to the accretion rates required to power quasars ($\sim 1\ M_\odot$ yr^{-1}). Therefore, an understanding of BAL outflows is required for an understanding of quasars as a whole. Usually BAL troughs are seen only in high-ionization species, but about 15% of BAL quasars also show absorption from low-ionization species, including absorption from excited fine-structure levels or terms of Fe II and Fe III in rare cases. In Hall et al. (2002, hereafter H02) we presented several examples of "overlapping-trough" BAL quasars whose flux shortward of Mg II is almost completely absorbed by troughs of excited Fe II (which is of course also accompanied by ground-state Fe II absorption). In this paper we present a high-resolution spectrum of one such object, SDSS J030000.56+004828.0 (hereafter simply SDSS J0300+0048) at $z = 0.89$, and use it to constrain the column densities and possible structure of its impressive outflow. SDSS J0300+0048 is only the fourth quasar known to have a Ca II BAL trough (see § 5.2.1 of H02)[13] and only the second to be studied at high resolution, after QSO J2359−1241

[1] Based on observations from ESO Director's Discretionary Time program 267.A-5698.

[2] Princeton University Observatory, Princeton, NJ 08544.
[3] Departamento de Astronomía y Astrofísica, Facultad de Física, Pontificia Universidad Católica de Chile, Casilla 306, Santiago 22, Chile.
[4] Research Associate, FNRS, University of Liège, Allée du 6 août 17, Batiment 5c, 4000 Liège, Belgium.
[5] European Southern Observatory, Casilla 19001, Santiago, Chile.
[6] Department of Astronomy, University of Washington, Box 351580, Seattle, WA 98195.
[7] Apache Point Observatory, P.O. Box 59, Sunspot, NM 88349-0059.
[8] Institute for Advanced Study, Olden Lane, Princeton, NJ 08540.
[9] Current affiliation: Steward Observatory, University of Arizona, Tucson, AZ 85721.
[10] Department of Astronomy and Astrophysics, Pennsylvania State University, University Park, PA 16802.
[11] Department of Astronomy and Astrophysics, University of Chicago, 5640 South Ellis Avenue, Chicago, IL 60637.
[12] Enrico Fermi Institute, University of Chicago, 5640 South Ellis Avenue, Chicago, IL 60637.

[13] Rupke, Veilleux, & Sanders (2002) find that ultraluminous infrared galaxies also can have Ca II outflows with large rest-frame equivalent widths (REWs). It is unclear how similar these narrower outflows are to Ca II BALs. The continuum around Ca II in most of their objects is dominated by galaxy light; the addition of a quasar continuum might greatly decrease the REWs. In any case, the outflows in SDSS J0300+0048 and QSO J2359−1241 have much larger blueshifts than the outflows studied by Rupke et al. (2002).

(Arav et al. 2001). Both quasars have "detached" absorption troughs that do not start at the systemic redshift: those in QSO J2359−1241 set in at a blueshift of ∼750 km s^{-1} and those in SDSS J0300+0048 at a blueshift of ∼1700 km s^{-1}. SDSS J0300+0048 also has a strong, narrow associated absorption system at the systemic redshift, with a Mg II REW of 1.882 Å. Whether this system is intrinsic to the quasar is one issue we consider in this paper.

We begin with a discussion of the most common method of analyzing intrinsic absorption lines, then apply this method to SDSS J0300+0048, and finally discuss our results.

2. ANALYZING INTRINSIC ABSORPTION LINES

Suppose we observe unblended doublet absorption from a BAL region covering a fraction C of the quasar's light with an optical depth τ. The resulting normalized residual intensities in the two lines of the doublet as a function of velocity v are

$$I_1(v) = 1 - C_v(1 - e^{-\tau_v}) , \quad (1)$$

$$I_2(v) = 1 - C_v(1 - e^{-R\tau_v}) , \quad (2)$$

where $R = g_2 f_2 \lambda_2 / g_1 f_1 \lambda_1$ is the ratio of the optical depth of line 2 to that of line 1 (the g_i are the statistical weights, the f_i are the oscillator strengths, and the λ_i are the wavelengths of the lines). Our convention is that I_1 refers to the stronger line of the doublet and τ_v refers to the optical depth in that line. For any doublet with $R = 0.5$, such as Mg II and Ca II, these equations yield the following solutions (Hamann et al. 1997) and associated uncertainties for C_v and τ_v:

$$C_v = \frac{1 + I_2^2 - 2I_2}{1 + I_1 - 2I_2} ,$$

$$\sigma_{C_v} = \frac{\sqrt{\sigma_{I_1}^2 (I_2 - 1)^4 + \sigma_{I_2}^2 [2(I_2 - 1)(2 + I_1 - 3I_2)]^2}}{(1 + I_1 - 2I_2)^2} \quad (3)$$

and

$$\tau_v = -\ln\left(\frac{I_1 - 1 + C_v}{C_v}\right) = -2\ln\left(\frac{I_2 - I_1}{1 - I_2}\right) ,$$

$$\sigma_{\tau_v} = \frac{2e^{\tau_v}(I_2 - I_1)}{(I_2 - 1)^2} \sqrt{\sigma_{I_1}^2 + \sigma_{I_2}^2 \left(\frac{I_1 - 1}{I_2 - 1}\right)^2} , \quad (4)$$

where it is understood that I_1 and I_2 are functions of velocity. The solution for C_v, and thus for τ_v as well, is physical ($0 \le C_v \le 1$) only when

$$0 \le I_1 \le 1 , \quad 0 \le I_2 \le 1 ,$$
$$I_2^2 \le I_1 , \quad I_2 \ge I_1 . \quad (5)$$

The last of the above conditions could be violated in the case of saturated absorption partially filled in by optically thin emission from the same doublet transition responsible for the absorption. The next to last could be invalidated by the presence in the spectrum of significant host galaxy or scattered quasar light.

The above equations can also break down if there are different covering factors for different emission regions (e.g., the continuum source, the broad emission line [BEL] region, and the Fe II emission region; see § 4.3.2 and Ganguly et al. 1999) or if the emissivities of the covered and uncovered regions are different functions of velocity (as pointed out by Srianand & Shankaranarayanan 1999 and observed by, e.g., Gabel et al. 2003). Moreover, the assumption that a fraction C of the quasar's light is occulted at a single optical depth τ and that the remaining light is unobscured is likely to itself be an approximation (de Kool, Korista, & Arav 2002b) and would be inappropriate if there are cases in which the resonance scattering interpretation of BAL quasars is correct (Branch et al. 2002). Nevertheless, the above equations are useful for studying BAL troughs, even if only to verify that one or more of the above complications is occurring.

If the absorption is broad enough that the two lines of the doublet are blended over a velocity width v_b that is less than their velocity separation Δv,[14] then there are three distinct velocity regimes to consider, which we label A to C from high velocity to low. In A and C one of the two lines produces blended absorption, while in B neither line is blended; see § 4.3.1 for a concrete example. Using positive v to denote outflows (absorption at shorter wavelengths) and assuming the stronger line (subscript 1) is the shorter wavelength one yield

$$\text{A}: \ v_{\max} > v > v_{\max} - \Delta v + v_b :$$
$$I_1 = 1 - C_v(1 - e^{-\tau_v}) , \quad (6)$$
$$I_2 = [1 - C_v(1 - e^{-R\tau_v})] \otimes [1 - C_{v-\Delta v}(1 - e^{-\tau_{v-\Delta v}})] ; \quad (7)$$
$$\text{B}: \ v_{\max} - \Delta v + v_b > v > v_{\max} - \Delta v :$$
$$I_1 = 1 - C_v(1 - e^{-\tau_v}) , \quad (8)$$
$$I_2 = 1 - C_v(1 - e^{-R\tau_v}) ; \quad (9)$$
$$\text{C}: \ v_{\max} - \Delta v > v > v_{\max} - \Delta v - v_b :$$
$$I_1 = [1 - C_v(1 - e^{-\tau_v})] \otimes [1 - C_{v+\Delta v}(1 - e^{-R\tau_{v+\Delta v}})] , \quad (10)$$
$$I_2 = 1 - C_v(1 - e^{-R\tau_v}) , \quad (11)$$

where $v_{\max}$ is the maximum outflow velocity and $C_{v\pm\Delta v}$ and $\tau_{v\pm\Delta v}$ are the covering factors and optical depths at velocities $v \pm \Delta v$. If blending does not occur ($v_b = 0$), regimes B and C vanish and regime A reduces to equations (1) and (2) because $C_{v\pm\Delta v}$ and $\tau_{v\pm\Delta v}$ become undefined—both C and τ will be defined only over a velocity range less than Δv. Otherwise, the convolution symbols indicate that the observed spectrum is affected by absorption from both lines in a possibly complicated manner. Nonetheless, because $C_{v\pm\Delta v}$ and $\tau_{v\pm\Delta v}$ are just the values of C_v and τ_v in regime B, which can be solved for, it may be possible to estimate the values of C_v and τ_v in regimes A and C. For example, if C_v is a constant and a fixed emission region is covered at all velocities, the convolutions are simple multiplications. This is not the case if C_v varies or if different emission regions are covered as a function of velocity, even if C_v is numerically constant.

3. VLT + UVES OBSERVATIONS OF SDSS J0300+0048

Observations of several SDSS BAL quasars were obtained on 2001 August 10–12 UT using the ESO Very

[14] See Junkkarinen, Burbidge, & Smith (1983) for an approach to the $v_b > \Delta v$ case.

Large Telescope (VLT) Unit 2 (Kueyen) and Ultra-Violet Echelle Spectrograph (UVES). This section provides observational details for all objects; science results for SDSS J2215−0045 and SDSS J1453+0029 can be found in Hall & Hutsemékers (2003) and for SDSS J0011+0055 in D. Hutsemékers et al. (2003, in preparation). A 1″ slit was used, yielding a resolution $R \simeq 40,000$ (7.5 km s^{-1}) at all wavelengths. A depolarizer was also used for all observations. Each exposure was reduced individually with optimum extraction (Horne 1986), including simultaneous background and sky subtraction. For SDSS J0300+0048, wavelengths 3030–3880 and 4760–6840 Å were observed simultaneously, in two exposures of 4500 and 2992 s, and wavelengths 3730–4990 and 6600–10600 Å simultaneously in a single exposure of 4500 s. Because the 3030–3880 Å setting had a very low signal-to-noise ratio and yielded different results for the two exposures, it is not used in this paper. The extraction for the 3730–4990 Å setting was determined manually in places where the flux was zero over several orders. Telluric absorption lines were removed for the red settings with the use of observations of telluric standard stars, shifted in velocity according to the different times of the observations and scaled in intensity according to the air mass difference. Whenever two or three exposures of each setting were available, their extracted spectra were averaged with rejection of cosmic rays and known CCD artifacts. Finally, all settings were rebinned to a constant wavelength interval of 0.015 Å on a vacuum heliocentric scale, scaled in intensity to match each other in their overlap regions and merged into a single spectrum.

4. ANALYZING SDSS J0300+0048

Figure 1 shows a portion of the SDSS spectrum of SDSS J0300+0048, intended to help put in context the small regions of high-resolution UVES spectra that we will present in this paper. From the central subsystem of the associated absorber seen in Ca II λ3969 and Mg I in the UVES spectrum, we adopt a systemic redshift of $z = 0.891850 \pm 0.000005$, in excellent agreement with the value of $z = 0.89191 \pm 0.00005$ measured from the narrow Mg II absorption in the SDSS spectrum (H02). There is weak [O II] emission at $z = 0.8908 \pm 0.0007$, which is a blueshift of 166 ± 111 km s^{-1} (using 3728.48 Å for the unresolved doublet's vacuum rest wavelength).

4.1. *What Is the Continuum?*

To analyze the absorption in SDSS J0300+0048 in a rigorously correct manner, we must know or be able to model its intrinsic, unabsorbed continuum at the wavelengths where absorption is present. Constructing such a continuum for the transitions of interest in SDSS J0300+0048 (Mg II, Mg I, and Ca II) requires the matching of complex blends of iron emission and absorption.

Figure 2 shows the SDSS rest-frame spectrum of SDSS J0300+0048 (*solid line*). The emission features longward of Mg II are plausibly identifiable as blends of Fe II and Fe I, as discussed in § 5.2 of H02, although we now recognize that Ti II emission is also likely to contribute (Kwan et al. 1995). The dashed line shows one possible model for the unabsorbed continuum of SDSS J0300+0048, consisting of a flat-in-F_λ power law plus a scaled and smoothed iron emission template. This template was constructed by fitting and subtracting a power law to the spectrum of the bright, narrow-lined, strong Fe II–emitting quasar SDSS J092332.33+574557.4 (D. P. Schneider et al., in preparation), using continuum windows at 1680–1700 and 3675–3710 Å. Because the template is intended for illustrative purposes only, no attempt was made to exclude emission from Mg II or

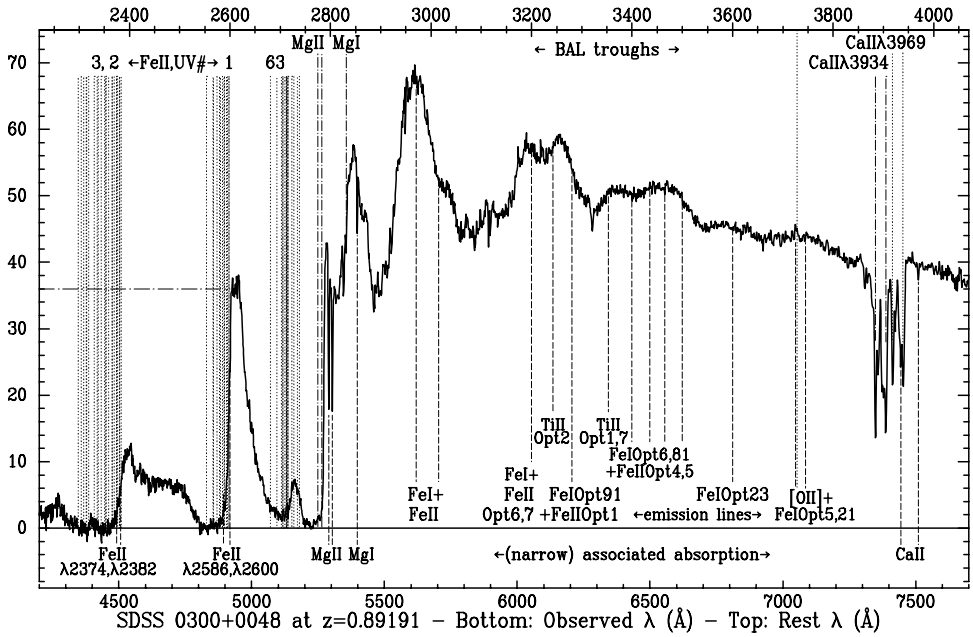

FIG. 1.—Portion of the SDSS spectrum ($R \sim 1800$) of SDSS J0300+0048 (F_λ in units of 10^{-17} ergs cm^{-2} s^{-1} Å^{-1} vs. λ). Selected broad absorption line troughs are labeled along the top, and the narrow associated absorption lines along the bottom, to help place the UVES spectrum in context. The likely emission lines are labeled just above the labels for associated absorption. The horizontal dot-dashed line shows the continuum level used to normalize the UVES spectrum shortward of 2600 Å rest frame. For a more comprehensive plot of the SDSS spectrum of this object, see H02.

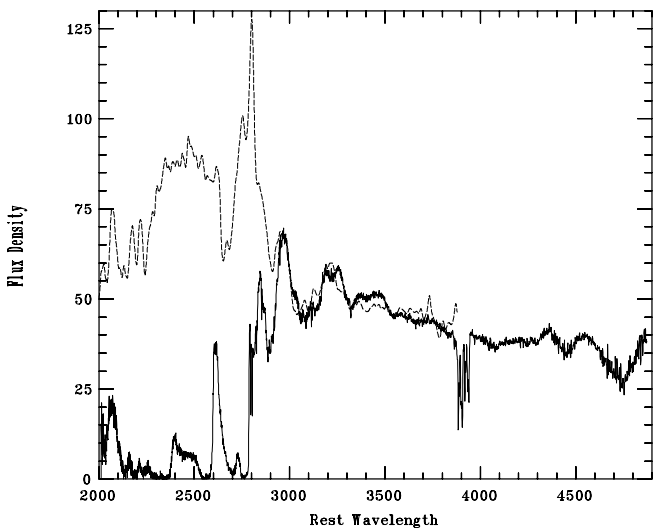

FIG. 2.—Flux density F_λ, in units of 10^{-17} ergs cm^{-2} s^{-1} Å^{-1}, of SDSS J0300+0048 (*solid line*) and a model for its intrinsic continuum (*dashed line*); see § 4.1.

other non-Fe transitions or to optimize the slope of the power-law continuum component of the model spectrum. This model spectrum is a good match to the emission feature just shortward of 3000 Å, the blue side of which may be affected by absorption, and to the wavelength extent of the weak feature at 3400–3600 Å. However, this latter feature is much stronger in SDSS J0300+0048 than in the model, SDSS J0300+0048 has emission features at 3025 and 3250 Å not seen in the model (the latter could be Ti II), and there are two features around 3100 Å in the template that are not seen in SDSS J0300+0048. Given these discrepancies between the model spectrum and the observed spectrum, we cannot use the model spectrum to predict the intrinsic continuum of SDSS J0300+0048 at $\lambda < 2900$ Å with any confidence. In the future it may be possible to find another strong Fe II–emitting quasar whose spectrum better matches that of SDSS J0300+0048 at $\lambda > 3000$ Å, but this is the best match we have found to date in the SDSS or in the literature (e.g., Graham, Clowes, & Campusano 1996). Note that the Fe emission templates of Boroson & Green (1992) and Vestergaard & Wilkes (2001) cover only 4250–7000 and 1250–3090 Å, respectively.

Alternatively, if we could match the $\lambda > 3000$ Å spectrum of SDSS J0300+0048 using a theoretical model, we could use that model to predict its unabsorbed continuum at $\lambda < 3000$ Å. However, published theoretical Fe II emission models either do not extend to $\lambda > 3200$ Å (Verner et al. 1999) or do not include sufficient transitions at $\lambda > 3200$ Å to match observations (Sigut & Pradhan 2003), and the situation for other possibly important ions such as Fe I and Ti II is no better.

Thus at present we have no reliable model for the unabsorbed continuum of SDSS J0300+0048 at the wavelengths of Mg II, Mg I, or Ca II. For Ca II, we can construct a reasonable local continuum. For Mg II, Mg I, and other transitions at even shorter wavelengths we must keep in mind that a local continuum estimate probably underestimates the unabsorbed continuum by a factor of ~2, unless dust reddening produces a turnover in the unabsorbed spectrum.

4.2. *The Associated Absorption*

To remove the narrow associated Ca II λ3934 blended with the broad Ca II λ3969, we must model the associated system. This procedure yielded interesting results, but ones tangential to the main paper, and so is discussed in the Appendix.

4.3. *The Broad Absorption*

4.3.1. *Overview*

Figure 3 shows the normalized spectrum of SDSS J0300+0048 around the broad absorption troughs of five separate transitions. The heavier lines denote spectral regions that are not confused with absorption from different transitions. Each transition has unique, unconfused velocity ranges, as we now discuss (Fig. 3, *top to bottom*).

The Mg II trough starts at about 1650 km s^{-1} and is at least 5500 km s^{-1} wide; Mg II is confused with Fe II λ2773 (UV63) above 7150 km s^{-1}. An upper limit to the Mg II trough width is impossible to determine, given that the continuum does not return to its unabsorbed level anywhere shortward of Mg II (Fig. 1). However, a reasonable maximum velocity can be inferred from the Fe II UV63 absorption, which disappears by ~10,850 km s^{-1} for the UV63 multiplet line with the shortest wavelength (2715 Å). That maximum velocity implies a Mg II trough at least 9200 km s^{-1} broad.

The Mg I absorption appears to start when the Mg II trough appears to saturate, at ~2000 km s^{-1}. It is unclear just how high a velocity the Mg I absorption reaches, both because Mg I is confused with associated Mg II above 5200 km s^{-1} and because the continuum normalization between Mg I and Mg II is very uncertain. The Mg I might reach only ~4000 km s^{-1}, matching the strong Ca II absorption, in which case the alternative continuum normalization shown by the tilted dashed line in the figure would be more appropriate. Alternatively, the Mg I might reach ~6400 km s^{-1}, matching the possible highest velocity Ca II, or even extend to above 7150 km s^{-1}—like Mg II—in which case it would overlap with Mg II.

The broad Ca II was normalized by a simple linear continuum fit to two narrow wavelength regions around 7294 and 7478 Å. To determine the blending in Ca II, we use the fact that Ca II λ3934 is the stronger line of the doublet, which means we can be sure that the highest velocity detectable absorption is from it and not from even higher velocity Ca II λ3969. The Ca II λ3934 absorption does not appear to reach velocities as large as the Mg II absorption does but instead disappears by ~5657 km s^{-1}. Given that the velocity separation of the Ca II doublet is 2640.1 km s^{-1}, the Ca II λ3934 trough is unblended only at 3017–5657 km s^{-1}. Similarly, because the Ca II λ3969 absorption starts at only 1697 km s^{-1}, the Ca II λ3969 trough is unblended only at 1697–4337 km s^{-1} (discounting the narrow associated Ca II λ3934 near 2640 km s^{-1}).

Ground-state Fe II absorption is undoubtedly present at all velocities where Mg II is seen, because the density and ionization conditions under which the two ions exist are very similar. However, at the lowest velocities in the outflow, the fine-structure levels of Fe II are not populated, and so excited Fe II absorption is not seen at those velocities, as first noted in H02. The Fe II λ2632 absorption (arising from an excited fine-structure level in the ground term; this is the longest wavelength line of the UV1 multiplet) is slightly

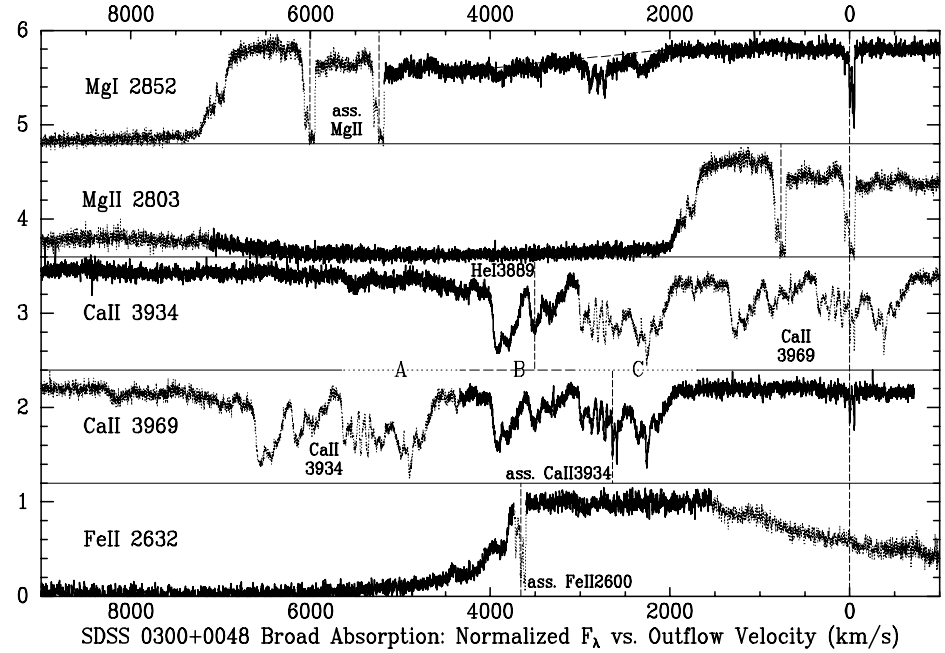

FIG. 3.—Normalized spectrum of SDSS J0300+0048 around the broad absorption troughs of five separate transitions. The spectrum of each transition is offset 1.2 units vertically from the one below it, with the thin solid lines showing the zero levels for each transition. Unconfused regions of the spectrum in each transition are shown with heavy lines. The velocity zero point is taken to be the redshift of the central component of the associated absorption system, and outflowing velocities are positive; thus, shorter wavelengths appear on the left. Velocity regimes A, B, and C are indicated between the Ca II λ3934 and Ca II λ3969 panels (see § 4.3). Dashed vertical lines show the locations of associated absorption; note that Fe II λ2600 but not Fe II λ2632 is seen in the associated absorber. The tilted dashed line in the Mg I panel shows an alternative continuum normalization.

contaminated by associated Fe II λ2600 (the strongest transition in the UV1 multiplet; this line is from the lowest fine-structure level in the ground term, not an excited level). Nonetheless, it is clear that the broad Fe II λ2632 absorption begins at a velocity that matches the highest velocity component of the main Ca II trough (see § 5.1). As mentioned earlier, the high-velocity limit of the Fe II absorption is at least 10,850 km s^{-1}.

All the above are low-ionization species, so at first glance it may seem surprising that they have different velocity distributions. However, the ionization potentials of Mg II and Fe II are higher than that of H I, while those of Mg I and Ca II are lower. This difference can lead to very different behavior for the latter two ions, as discussed in § 5.2.

4.3.2. *Broad* Ca II *Absorption: Velocity Regime B*

To begin the quantitative analysis of the broad Ca II absorption, we used equations (8) and (9) to solve for C_v and τ_v in the unblended outflow at 3017–4337 km s^{-1} (velocity regime B). The results are shown in Figure 4, where the original pixels have been binned by a factor of 5 in order to achieve an acceptable signal-to-noise ratio (S/N). We defer a detailed discussion of this figure until later in this section. Note that no points are plotted for velocity bins where the residual intensities do not allow a physical solution because one or more of the conditions of equation (5) are violated. This situation occurs for 37% of the original pixels in velocity regime B. Inspection of the velocities where the residual intensities did not allow a physical solution suggested that our continuum normalization was an underestimate. Thus we refitted the continuum using a third-order Legendre polynomial between two narrow wavelength regions around 7278 and 7496 Å. This normalization yielded only a slight

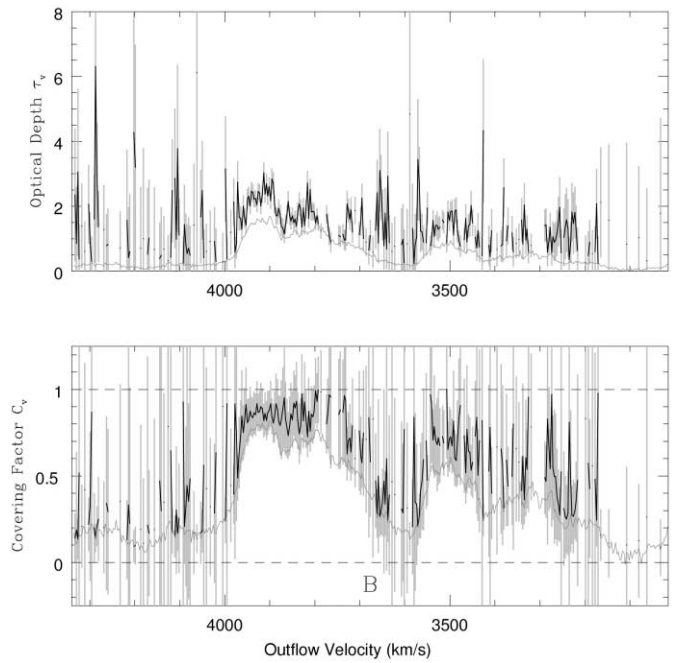

FIG. 4.—The thick black line gives the optical depth (*top*) and covering factor for Ca II as a function of velocity in the (unblended) velocity regime B, after binning by 5 pixels in the dispersion direction. Points are plotted only when a physical solution is possible at that velocity. The gray areas show the ± 1 σ uncertainty ranges, which can exceed the range of physical solutions (namely, $0 \leq C_v \leq 1$, shown by the dashed lines in the bottom panel). The thin gray line in the top panel shows the minimum optical depth needed to match the observed Ca II λ3934 absorption in the limit of 100% covering. The thin gray line in the bottom panel shows the minimum covering factor needed to match the observed Ca II λ3934 absorption in the limit of infinite optical depth. See § 4.3.2 for discussion. [*See the electronic edition of the Journal for a color version of this figure.*]

increase in the number of pixels where the residual intensities allowed a physical solution, suggesting that our continuum normalization is not the major source of error in that respect.

One possible source of error is scattered light or host galaxy light that does not pass through the BAL region and thus fills in the absorption troughs. Host galaxy light should be a $\lesssim 1\%$ effect because this quasar is quite luminous ($M_i = -27.08$ for $H_0 = 70$ km s^{-1} Mpc^{-1}, $\Omega_M = 0.3$, and $\Omega_\Lambda = 0.7$; D. P. Schneider et al., in preparation). The observed minimum residual intensity in the broad Ca II trough is $6.0\% \pm 1.5\%$ of the continuum, so that is the maximum percentage that unabsorbed scattered light or host galaxy light can contribute to the observed continuum. To test the effects of a maximal contribution from unabsorbed scattered light, we subtracted 0.06 from the residual intensity at all velocities, renormalized by 0.94, and repeated our calculation of C and τ. This adjustment slightly decreased the number of pixels with allowed physical solutions, suggesting that ignoring the contribution of scattered light does not greatly affect the calculation of C_v and τ_v.

Another possible source of error is our assumption that the covering factor is the same for the featureless continuum source and Fe II emission regions. Doublet absorption does not provide enough information to solve for two covering factors independently. However, § 4.2 of Ganguly et al. (1999) discusses how joint constraints on C_c and $C_{\rm Fe}$ can still be made, given the ratio W of the Fe II flux to the continuum source flux. For a lower limit of $W = 0.07$ in SDSS J0300+0048, the situation lies in between that of a single covering factor and the scattered light case considered previously, so assuming a single covering factor is reasonable. In the more realistic $W = 0.27$ case, the covering factors have similar, large values (maxima of $C_c > 0.92$ and $C_{\rm Fe} > 0.72$), and assuming a single covering factor again appears reasonable.[15]

Neither the details of the assumed continuum, the neglect of scattered light, or the assumption of a single covering factor appears responsible for the relatively large fraction of pixels (37%) for which the residual intensities in the Ca II doublet lines do not allow a physical solution for C_v and τ_v. The explanation for these pixels must lie primarily in the random noise. This explanation is consistent with Figure 4, which shows that the bulk of the pixels without physical solutions lie in the regions of weak absorption, where the noise is comparable to the strength of the absorption. (The average S/N per pixel in the Ca II trough is 17, with a range between 8 and 24.)

Considering Figure 4 in more detail, we see that in many individual velocity bins (each consisting of 5 original pixels) both the minimum C_v solution (*thin gray line*) and the $C_v = 1$ solution are formally acceptable at the 68% confidence level ($\pm 1\ \sigma$). However, the lower panel of Figure 4 shows that overall the covering factor in the unblended outflow is statistically inconsistent with both limiting cases. Neither $C_v = 1$ at all velocities nor C_v having its minimum value at all velocities is a good fit to the data as a whole. The upper panel corroborates the conclusion that the uniform $C_v = 1$ solution is unacceptable: that solution corresponds to τ_v having its minimum value at all velocities, whereas the best-fit optical depth is consistently larger than the minimum.

4.3.3. *Broad* Ca II *Absorption: Velocity Regime A*

To model the Ca II λ3934 absorption in velocity regime A (4337–5657 km s^{-1}), we extrapolate from the absorption at 4000–4337 km s^{-1} in velocity regime B. The absorption there, while noisy, is much more consistent with the minimum C_v than with $C_v = 1$, and the optical depth is consistent with being constant at its weighted average of $\tau_v = 0.88 \pm 0.03$. We adopt a fixed $\tau_v = 0.88$ for regime A, which means that the corresponding fractional absorption in Ca II λ3969 is 61% of that in Ca II λ3934 and that the covering factor C_v is 1.71 times its minimum possible value at each v. We also calculate the limiting minimum-C_v and $C_v = 1$ cases, as they delimit the range of plausible systematic errors.

4.3.4. *Broad* Ca II *Absorption: Velocity Regime C*

To the observed residual Ca II λ3934 intensities in this velocity range, we add back in the fractional absorption in high-velocity Ca II λ3969 estimated in the previous section. We then solve for C_v and τ_v as per usual. Figure 5 shows the results. The uncertainty ranges shown as the gray areas include the systematic uncertainties arising from the removal of the high-velocity Ca II λ3969. Note that the removal of high-velocity Ca II λ3969 resulted in a large increase in the number of pixels in this velocity regime with valid physical solutions.

In most velocity bins, the minimum C_v solution cannot be ruled out but the $C_v = 1$ solution can. On average, however, C_v is significantly larger than the required minimum value.

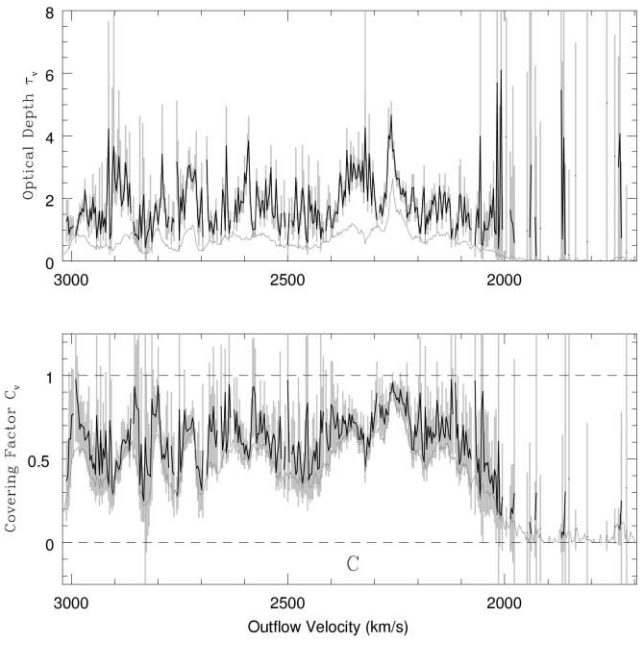

FIG. 5.—Optical depth (*top*) and covering factor for Ca II as a function of velocity in the (blended) velocity regime C, after binning by 5 pixels in the dispersion direction. Symbols are as in Fig. 4. The uncertainty ranges (*gray areas*) include the systematic uncertainties from the assumptions made in order to remove the blended absorption, but the random errors almost always dwarf the systematic uncertainties. See § 4.3.4 for discussion. [*See the electronic edition of the Journal for a color version of this figure.*]

[15] We cannot rule out an Fe II emission region that remains uncovered until the continuum emission region is fully covered and thus has $C_{\rm Fe} = 0$ at most velocities. However, refitting C_v and τ_v for such a scenario yields a large increase in the number of pixels that does not correspond to a physical solution.

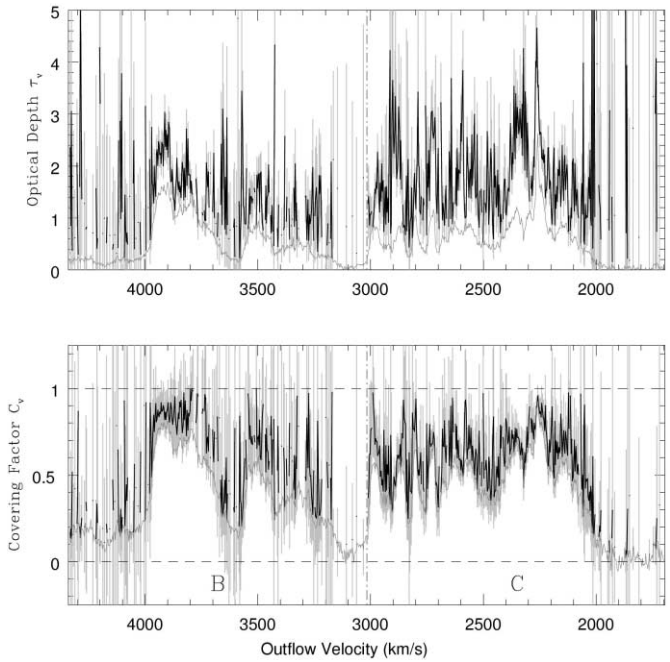

FIG. 6.—Optical depth (*top*) and covering factor as a function of velocity for the Ca II absorption, after binning by 5 pixels in the dispersion direction. Note that the optical depth scale is different than in the previous two figures. The vertical dot-dashed line at 3017 km s^{-1} separates velocity regimes B and C; other symbols are as in Fig. 4. See § 4.3.5 for discussion. [*See the electronic edition of the Journal for a color version of this figure.*]

This behavior is similar to that in velocity regime B, although not as pronounced.

4.3.5. *Broad* Ca II *Absorption: Summary*

Figure 6 shows the optical depth and covering factor over the velocity range of strong Ca II absorption. As mentioned previously, the covering factor is on average significantly greater than the minimum value, although it tracks the minimum value more closely in velocity regime C than in regime B. The Ca II outflow is moderately saturated ($1 < \tau < 3$), with only one significant spike above 4. Thus, in general, the covering factor determines much—but not all—of the shape of the absorption profile in the Ca II outflow.

4.3.6. *The Broad* Mg I λ2852 *Absorption*

As seen in Figure 3, the strongest Mg I absorption in the broad outflow is present between 2000 and 3000 km s^{-1}. Figure 7 shows the absorption and Ca II optical depth over this velocity range in detail. Not all the fluctuations in τ_v are real, of course, but the five high-τ features marked with the dotted lines are statistically significant. (The lone high-τ feature near 2600 km s^{-1} is likely a residual from the correction of blended associated absorption in the Ca II λ3969 trough.) The two features between 2200 and 2400 km s^{-1} have weak Mg I. The three narrow absorption features between 2700 and 2900 km s^{-1} have a larger Mg I/Ca II ratio because they have equal or smaller $\tau_{\rm Ca\,II}$ (and similar σ_τ) but stronger Mg I absorption.[16]

[16] The three features are seen in both Mg I and Ca II, but the velocity distributions of their absorption strengths differ in two features. The $\tau_{\rm Ca\,II}$ does match the depths of the Mg I features rather well, however, suggesting that Mg I is unsaturated while the large τ_v and variable C_v in Ca II shift its velocity centroid away from that of Mg I.

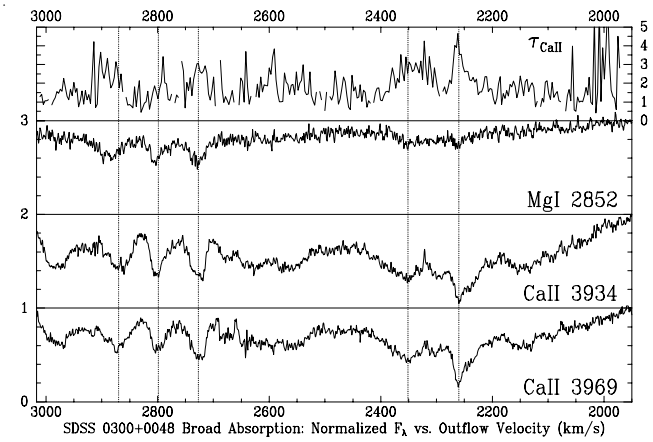

FIG. 7.—Close-up of velocities where strong Mg I absorption is present in the BAL outflow. The uppermost panel and right-hand scale show the Ca II λ3934 optical depth. The lower three panels show normalized intensities in the Mg I λ2852, Ca II λ3934, and Ca II λ3969 regions, the latter corrected for narrow, blended associated Ca II λ3934. The Mg I region normalization is uncertain, as it is unclear whether there is Mg I absorption at 2400–2700 km s^{-1}. See § 4.3.6 for discussion.

Note that there is no evidence for any features in the (heavily saturated) Mg II trough at these velocities, nor is there any sign of Ca I λ4227.9 absorption. As with those in the associated absorber (see the Appendix), these Mg I/Ca II ratio variations seem likely to be due to metallicity or abundance variations, although CLOUDY modeling is needed to firmly rule out an ionization parameter effect. The striking similarity of the features in the Mg I and Ca II troughs rules out the possibility that the two ions are found in physically distinct regions that happen to share the same velocity.

A similar effect may be present in QSO J2359−1241. Table 1 of Arav et al. (2001) shows that its absorption component e has a Ca II/Mg I ratio several times larger than that in components b and c. Unlike in SDSS J0300+0048, the broader component (e) has the higher Ca II/Mg I ratio. However, the spectra of Arav et al. (2001) included only one line of the Ca II doublet, so the reality of the Ca II/Mg I variation in QSO J2359−1241 remains to be confirmed.

4.3.7. *Column Densities in the BAL Outflow*

For an ion giving rise to unsaturated and instrumentally well-resolved doublet absorption, the optical depth at velocity v is directly proportional to the column density per unit velocity at v, N_v, which has units of cm^{-2} (km s^{-1})$^{-1}$ (Savage & Sembach 1991). The total column density (Arav et al. 1999) and its uncertainty, both in units of cm^{-2}, are then given by

$$N = \int N_v dv = \sum N_v \Delta v = \frac{3.7679 \times 10^{14}}{\lambda_1 f_1} \sum \tau_v \Delta v \ ,$$
$$\sigma_N = \frac{3.7679 \times 10^{14}}{\lambda_1 f_1} \sqrt{\sum (\sigma_{\tau_v} \Delta v)^2} \ , \qquad (12)$$

where we have ignored the uncertainties on the wavelength λ_1 (in Å) and the dimensionless oscillator strength f_1 of the stronger line of the doublet, which has optical depth τ_v in the velocity bin of width Δv (in km s^{-1}) at velocity v.[17] For saturated absorption, equation (12) yields a lower limit to

[17] N and N_v are independent of the covering factor C_v, but the total mass present in that ion along the line of sight does depend on C_v.

TABLE 1
COLUMN DENSITIES IN THE SDSS J0300+0048 BAL OUTFLOW

ION	VELOCITY RANGE			
	1697–3740 km s^{-1}	3740–5657 km s^{-1}	5657–8221 km s^{-1}	Total
Fe II*	$\leq(0.04 \pm 0.16) \times 10^{15}$	$\geq(1.34 \pm 0.09) \times 10^{15}$	$\geq(2.95 \pm 0.58) \times 10^{15}$	$\geq(4.29 \pm 0.59) \times 10^{15}$
Mg II	$\geq(1.90 \pm 0.34) \times 10^{15}$	$\geq(2.51 \pm 0.09) \times 10^{15}$	$\geq(2.20 \pm 0.07) \times 10^{15}$	$\geq(6.61 \pm 0.36) \times 10^{15}$
Mg I	$\geq(1.54 \pm 0.02) \times 10^{13}$[a]	$\geq(2.84 \pm 0.02) \times 10^{13}$	...	$\geq(4.38 \pm 0.03) \times 10^{13}$[a]
He I*	$\leq 2.5 \times 10^{14}$	$\leq 2.3 \times 10^{14}$	$\leq 3.1 \times 10^{14}$	$\leq 7.9 \times 10^{14}$
Ca II	$(5.22 \pm 0.75) \times 10^{14}$	$(1.91 \pm 0.87) \times 10^{14}$	$\leq(0.3 \pm 1.2) \times 10^{12}$	$(7.13 \pm 1.15) \times 10^{14}$
Ca I	$\leq 0.2 \times 10^{12}$	$\leq 0.8 \times 10^{12}$	$\leq 0.7 \times 10^{12}$	$\leq 1.7 \times 10^{12}$

NOTE.—All column densities are given in units of cm^{-2}. The asterisks in the first column denote ions whose column densities are measured in excited states rather than the ground state.

[a] This Mg I column density is a conservative lower limit; more liberal assumptions yield almost exactly the same column density as at 3740–5657 km s^{-1}. In that case, the total Mg I column would be $(5.66 \pm 0.03) \times 10^{13}$ cm^{-2}.

the true N. For a singlet transition with $C_v = 1$, $\sigma_{\tau_v} = \sigma_1 e^{\tau_v} = -\sigma_1/I_1$. In our calculations of N for various ions, at velocities where τ_v or σ_{τ_v} are formally undefined, we linearly interpolate using the two nearest defined values. For singlet transitions, for velocities where τ_v is formally undefined, we assume that $\tau_v = -\ln(I_1)$, even if the result is a negative τ_v.

We are interested in the column densities in three different velocity regimes, which are not quite the same as the Ca II regimes ABC. First is 1697–3740 km s^{-1}, where the Ca II absorption is strong but excited Fe II absorption is absent. Next is 3740–5657 km s^{-1}, where both Ca II and excited Fe II absorption are present. Last is 5657–8221 km s^{-1}, where Ca II is absent but Mg II and excited Fe II remain relatively unconfused. The column densities we derive for the various ions in these velocity regimes are listed in Table 1 and are discussed below. We do not measure column density limits for the additional ~2600 km s^{-1} of Mg II and excited Fe II absorption present above 8221 km s^{-1} (§ 4.3.1).

We find a total $N_{\rm Ca\,II} = (7.13 \pm 1.15) \times 10^{14}$ cm^{-2}. For Ca I λ4227.9 we assume $C_v = 1$ to set a limit of $N_{\rm Ca\,I} \leq 1.7 \times 10^{12}$ cm^{-2} for the entire outflow.

We set a rough lower limit on $N_{\rm Mg\,II}$ by ignoring Mg II λ2803 and summing only Mg II λ2796, assuming $C_v = 1$ and thus $\tau_v = -\ln(I_v)$, where I_v is the residual intensity at velocity v. This yields $N_{\rm Mg\,II} \geq (6.61 \pm 0.36) \times 10^{15}$ cm^{-2} (for 1697–8221 km s^{-1}). Normalizing by the strong Fe II emitter continuum shown in Figure 2, which is ~2 times larger than the continuum we have assumed, would increase τ by only ~log(2) and $N_{\rm Mg\,II}$ by only ~20%–25%. However, because the Mg II trough is strongly saturated, the value of $N_{\rm Mg\,II}$ is a lower limit regardless of the continuum chosen.

For Mg I we set a conservative lower limit by assuming $C_v = 1$, normalizing by the dashed line in Figure 3, and summing over $v = 2000$–4500 km s^{-1}. This yields $N_{\rm Mg\,I} \geq (1.73 \pm 0.02) \times 10^{13}$ cm^{-2}. A more liberal estimate, obtained using the default normalization shown in Figure 3, yields $N_{\rm Mg\,I} \geq (5.66 \pm 0.03) \times 10^{13}$ cm^{-2} for 1697–5157 km s^{-1}, beyond which Mg I is confused with Mg II. Alternatively, using the strong Fe II emitter continuum would increase the lower limit on $N_{\rm Mg\,I}$ by $\Delta N_{\rm Mg\,I} = 1.1 \times 10^{14}$ cm^{-2}. Clearly, the systematic uncertainty in the continuum placement is the major uncertainty.

As for excited He I (He I* for short), there is a possible detection of weak ($\lesssim$5% of the continuum), broad He I λ3188 absorption, but this line lies atop a broad emission complex, and so the continuum normalization is quite uncertain. Also, despite confusion with Ca II λ3934, we see no sign of He I λ3889 absorption with depth more than ~5% of the continuum (Fig. 3), even though its optical depth is 3 times that of He I λ3188. He I λ2945 provides no useful constraints because the observed continuum surrounding it is simply too complex to be normalized accurately. It is possible that there is saturated He I* absorption from a region with $C_v \lesssim 0.05$, but we are most interested in limits on He I* at velocities where Ca II or Mg II absorption is seen, and such absorption has $C_v \gg 0.05$. To estimate a limit on $N_{\rm He\,I*}$, we assume absorption 5000 km s^{-1} wide with $C_v = 1$, $\tau_{3188} = 0.02$, and $\tau_{3889} = 0.06$, which yields $N_{\rm He\,I*} \leq 4.6 \times 10^{14}$ cm^{-2}.

Our upper limit on the excited Fe II column (Fe II* for short) at 1697–3740 km s^{-1} comes from the nondetection of Fe II λ2632, which is a blend of two lines. Using NIST database $g_i f_i$ values for these lines from de Kool et al. (2001), we find $N_{\rm Fe\,II*} \leq (0.42 \pm 1.62) \times 10^{13}$ cm^{-2}. Our lower limits on the excited Fe II column at higher velocities come from assuming $C_v = 1$ and attributing the absorption to a blend of all lines from Fe II multiplet UV1 at 2618–2633 Å, a velocity span of 1600 km s^{-1}. We used NIST database $g_i f_i$ values from de Kool et al. (2001) for those lines as well. An exact accounting of which lines contribute at which wavelengths would change the calculated lower limit somewhat, but the saturated absorption means the column density is probably much greater than the lower limit anyway. We do not attempt to convert these limits on the Fe II column in states ~0.1 eV above ground to limits on the total Fe II column.

The above column densities could be underestimates if features in the outflow are barely resolved at our velocity resolution. If this is the case, recalculating the column densities after binning the spectrum will yield significantly smaller values. We find this to be only a ~10% effect: the Ca II column densities calculated from the spectrum after binning by 5 pixels are about 15% lower than the unbinned values in velocity regime B and 5% lower in velocity regime C.

5. DISCUSSION

5.1. *Broad* Ca II *Absorption versus Broad, Excited* Fe II *Absorption*

It is worth reiterating the interesting fact that the BAL region responsible for the main Ca II trough also produces Mg I and Mg II absorption but none from excited Fe II,

except for a small velocity range at the highest velocities where Ca II is seen (§ 4.3.1 and Fig. 3). Presumably the Ca II region does produce ground-state Fe II absorption, but such absorption cannot be studied because it is blended with higher velocity excited Fe II.

Because the true continuum at the wavelengths where we expect to see excited Fe II absorption from the Ca II–absorbing gas is likely much higher than we have assumed (Fig. 2), there is almost certainly some absorption present at those wavelengths. Nonetheless, we can rule out the possibility that excited Fe II is present at 2000–3500 km s^{-1} with non-black saturation. For that to be the case, the unabsorbed continuum at the velocities in question would have to be higher than we have assumed by a factor equal to the inverse of the partial covering. The Ca II absorber reaches $C_v \simeq 0.95$ in this velocity range, thus requiring for this scenario an unabsorbed continuum 20 times higher than assumed. However, a continuum only factor of 2 higher is expected at rest 2600 Å even if the true continuum is that of a strong Fe II emitter (Fig. 2).

One possible explanation for the different velocity distributions of Ca II and excited Fe II is that the Ca II region has a density that is too low for collisional excitation to significantly populate excited states of Fe II ($n_e < 10^3$ cm^{-3}; de Kool et al. 2001); at such densities radiative excitation will not contribute significantly either (§ 4.1.3 of Wampler, Chugai, & Petitjean 1995). Alternatively, the Ca II could arise from a region with a density similar to that in the Fe II region, but with a lower temperature. The levels that give rise to Fe II $\lambda\lambda$2632 absorption have an average excitation potential of 0.095 eV, so a temperature $T \lesssim 1100$ K is required to avoid populating them significantly. Absorption from the somewhat weaker Fe II λ2626 line is not detected either, and its excitation potential is only 0.048 eV. Thus the temperature could be as low as $T \lesssim 550$ K in the Ca II region. Which of these alternatives—low density or low temperature—is most likely the case for the Ca II region depends on the structure of the outflow, as we now discuss.

5.2. *Column Densities and Outflow Models*

Compared with QSO J2359−1241 (Arav et al. 2001), the only other Ca II BAL quasar studied at high resolution, SDSS J0300+0048 has lower limits on the total Mg I and Mg II column densities ∼30 times larger, a lower limit on the excited Fe II column ∼95 times larger, an upper limit on the excited He I column ∼8 times larger, and a total Ca II column ∼200 times larger. The column densities for all but the excited Fe II are the largest reported to date in any BAL outflow.

These values are consistent with the total column density of metals being ∼200 times larger in SDSS J0300+0048 than in QSO J2359−1241. The excited He I column need not increase as much because it comes from the He II region instead of the low-ionization BAL region that produces most of the absorption in SDSS J0300+0048. Also, the excited He I absorption can be greatly reduced if the He II region has an n_e below the critical density for this excited state (3×10^3 cm^{-3}).

Arav et al. (2001) found that the absorption in QSO J2359−1241 could be explained by solar-metallicity gas with $\log N_H \simeq 20$ and $\log U \simeq -3$. The existence of a hydrogen ionization front requires a column density $N_H \simeq U \times 10^{23}$ cm^{-2} (Davidson & Netzer 1979), or a few times larger than that for electron densities $n_e \gtrsim 10^{9.5}$ cm^{-3} (de Kool et al. 2002a). QSO J2359−1241 has just enough column density to have a hydrogen ionization front ($\tau \sim 2.5$ at the Lyman limit). The ∼200 times larger Ca II column density in SDSS J0300+0048 means that it must have a strong hydrogen ionization front. Even if SDSS J0300+0048 is one of the most metal-rich quasars known, with metallicity ∼15 times solar (Baldwin et al. 2003), it would have to have a Ca II region with $N_H \sim 13$ times larger than in QSO J2359−1241, corresponding to $\tau \sim 33$ at the Lyman limit.

The presence of an H I ionization front in SDSS J0300+0048 agrees with expectations from photoionization calculations (Ferland & Persson 1989). An H I ionization front surrounding the quasar[18] can shield Mg II and Fe II from ionization (Voit, Weymann, & Korista 1993). However, such a front by itself cannot protect Mg I or Ca II: because those ions have lower ionization potentials than H I, they are found only where the ionization parameter is low (Hamann et al. 2001). Mg I can be found in low-ionization gas with total column density less than, or just equal to, that needed for an H I ionization front (Arav et al. 2001); Ca II cannot, due to resonant photoionization from the lowest metastable level of Ca II by Lyα photons (Joly 1989). Thus, Ca II exists only well outside an H I front, where not just the ionization parameter but also the densities of Lyα photons and photons with $E > 11.9$ eV—required to ionize Ca II—are all low. In fact, for the clouds of density $10^{9.5}$ cm^{-3} modeled by Ferland & Persson (1989), Ca II becomes the dominant ionization stage of calcium only behind the C I ionization front, at a column density more than a factor of 10 higher than that of the H I ionization front.

This requirement has implications for the structure of the outflow, because it means that the excited Fe II BAL region cannot be farther from the quasar than the Ca II BAL region. If it was, it would lie outside the H I ionization front and would also show strong Ca II absorption. (The weak Ca II absorption from the excited Fe II region means that at most $\lesssim 10\%$ of the excited Fe II–absorbing gas could lie outside the front.) This fact, along with the observations that the broad absorption is detached from the systemic redshift and that the Ca II BAL region lies at low velocities (1697–3740 km s^{-1}) while the excited Fe II BAL region lies at high velocities (3740–8221 km s^{-1} and beyond), enables us to constrain which of two representative, competing BAL outflow models might explain SDSS J0300+0048. These models are the disk wind model of Murray et al. (1995) and a model in which the absorption arises in confined clouds embedded with very small filling factor in a less dense, hotter medium (e.g., Arav & Li 1994). Such clouds could form a dusty outflow that nearly surrounds the quasar (e.g., Becker et al. 2000), or they could be "ablated" from denser sources, such as an accretion disk or obscuring torus, and block only some lines of sight to the quasar.

In the radiatively driven disk wind model of Murray et al. (1995), the streamlines of the outflow begin at some angle to the disk and then bend to become asymptotically radial (in radial cross section). Thus the detachment velocity simply reflects the height above the disk reached by the flow before it crosses the line of sight to the continuum source; that

[18] The ionization front is centered on the quasar, so we use the terms "inside" and "outside" the front instead of "in front of" and "behind" the front.

height could be different for different ions. As the distance from the quasar increases *along a single streamline*, the velocity and ionization increase and the density decreases. For *two* streamlines arising at *different* initial radii, the more distant streamline will be scaled up in density (Shakura & Sunyaev 1973) but down in velocity and ionization parameter (Murray et al. 1995). Because we see a detached flow in SDSS J0300+0048, in this model our line of sight must cross numerous streamlines. Thus, we expect to see higher velocity gas that is less dense, more highly ionized, and located at smaller radii.[19]

The BAL outflow in SDSS J0300+0048 is consistent with such a disk wind, as the lowest ionization gas (traced by Ca II and Mg I) is found at the lowest velocities. To be consistent with the observed anticoincidence of excited Fe II absorption and Ca II absorption requires that a disk wind in SDSS J0300+0048 have $n_e > 10^3$ cm^{-3} throughout but $T \lesssim 1100$ K at the low velocities (large radii) where Ca II is present. If the velocity decreases monotonically with radius along the line of sight, then the H I ionization front will shield gas at all velocities less than some velocity v_s. Because the Ca II absorption can arise only outside the H I ionization front, we surmise either that $v_s \simeq 5750$ km s^{-1}, which is the maximum observed Ca II velocity, or that $v_s \simeq 4000$ km s^{-1}, which divides strong and weak Ca II absorption, and that the higher velocity Ca II absorption is due to a small portion (by mass) of the outflow departing from a monotonically decreasing velocity. If the Mg II trough were not saturated, it might reveal the velocity of the front, as the ionic fraction of Mg II increases sharply outside the front (Voit et al. 1993).

If we try to explain the Ca II absorption as arising from clouds with a lower density than the clouds giving rise to excited Fe II absorption, but at similar radii, then the Ca II BAL clouds must have $n_e < 10^3$ cm^{-3} while the excited-Fe II BAL clouds have a higher n_e and lower T, assuming all clouds are in pressure balance with the same confining medium. However, the column density in the Ca II clouds must be larger than that in the excited-Fe II BAL clouds, which leads to an improbable scenario in which diffuse clouds reach high column densities but dense clouds do not.

Thus, as in the disk wind case, we are driven to a scenario in which the excited Fe II BAL clouds must have $n_e > 10^3$ cm^{-3} while the Ca II BAL clouds have an even higher n_e but a temperature $T \lesssim 1100$ K, to avoid populating the excited Fe II levels.

For a cloud scenario in which the outflow surrounds the quasar, the outflow must have smaller velocities at larger radii because the Ca II BAL region must lie at larger radii than the excited Fe II BAL region. This velocity distribution might occur if this quasar recently "turned on" inside a relatively thick shell or torus of gas and has gradually radiatively accelerated (and radially compressed) it such that the velocity in the shell is a decreasing function of radius. The Ca II absorption would arise in the outermost regions of the flow, which have been accelerated only to velocities of $\sim$2000–4000 km s^{-1} so far. This scenario is rather contrived, especially as such an outflow will be Rayleigh-Taylor unstable (although magnetic fields might suppress the instabilities), but it can be tested by looking for a long-term increase in the velocity of the Ca II BAL outflow.

A cloud scenario in which the outflow does *not* surround the quasar can explain the detached troughs by positing that the injection points of the clouds (where they have $v_{\rm radial} = 0$) do not lie along our line of sight to the continuum source and that there is some finite outer radius for the injection that corresponds to the minimum radial velocity we observe. Thus the outflow cannot be spherically symmetric, as such a flow would have injection points along all lines of sight. Injection of clouds from a disk or torus is still feasible. The clouds must cross our line of sight in a spatially and velocity-segregated flow, as in the disk wind case, because the (low velocity) Ca II–absorbing clouds must be at larger radii than the (high velocity) Fe II–absorbing clouds. If clouds of all velocities were intermixed, the gas in any high-velocity clouds shadowed by a low-velocity Ca II–absorbing cloud would recombine to lower ionization states on timescales of $\sim 10^{11}/n_e$ seconds. The result would be Ca II absorption at high velocities as well as low, which is not seen.

Thus, for a cloud model to explain this outflow, the clouds must form either a rather contrived expanding shell or a segregated flow arising from a disk or torus. The latter case differs from the disk wind model only in the presence of an intermixed, hot, confining medium for the gas responsible for the low-ionization absorption.

Finally, it is not clear how the associated absorption fits into either the cloud or the disk wind model. However, in both models it must arise far enough from the continuum source that it has not been significantly accelerated along our line of sight. Another of the five overlapping-trough BAL quasars in H02, SDSS J0819+4209, has BAL troughs detached from an AAL system. That object has a similar detachment velocity ($v = 2180 \pm 80$ km s^{-1}), but the Mg II AAL appears to be broader than in SDSS J0300+0048. Anecdotally, AALs and detached BALs appear to be common in additional overlapping-trough quasars being found by the SDSS, but the possible significance of this finding to models of these outflows remains unclear.

6. CONCLUSION

Comparison with QSO J2359−1241, the only other Ca II BAL quasar studied at high resolution, suggests that the outflow in SDSS J0300+0048 has a strong H I ionization front, in agreement with the photoionization modeling of Ca II by Ferland & Persson (1989). The observed Ca II absorption must arise in low-ionization gas located outside the ionization front. Kinematically, the outflow is detached—it begins only at a velocity blueshifted by $\sim$1700 km s^{-1} from the associated absorption redshift. Furthermore, excited Fe II absorption is seen only at high velocities, and strong Ca II absorption only at the low velocity end of the outflow.

The velocity and ionization structure in the SDSS J0300+0048 outflow can be explained in a disk wind model where the Ca II arises only at large radii. A cloud model for the BAL outflow can explain the observations if the clouds form a segregated flow originating from a source out of our

[19] The simulations of Proga, Stone, & Kallman (2000) verify these analytic predictions of Murray et al. (1995) for radiatively driven disk winds. These predictions are less secure in the magnetohydrodynamic simulations of Proga (2003), which yield a turbulent zone of considerable solid angle between the fast radiatively driven wind component and a slower MHD component that develops closer to the equatorial plane. Should the line of sight pierce that latter zone, the relationship between velocity, density, ionization parameter, and distance may break down.

line of sight—in other words, a clumpy disk wind instead of a smooth one (e.g., Everett 2003). An outflow of clouds that completely surrounds the quasar can explain the observations only in the case of a shell of gas in which the velocity decreases with increasing radius and in which the gas has been uniformly accelerated such that none of it has velocities $v \lesssim 1700$ km s^{-1}. While this model is rather contrived, it is testable because it predicts a long-term increase in the observed velocity of the outflow.

The region producing excited Fe II absorption must have $n_e > 10^3$ cm^{-3} and $T \gtrsim 1100$ K to significantly populate the observed fine-structure levels. In any of these models, it is almost certain that the region producing Ca II absorption also has $n_e > 10^3$ cm^{-3}, in which case the Ca II–absorbing region must have $T \lesssim 1100$ K—and perhaps as low as $T \lesssim 550$ K—to prevent excited Fe II states from being populated there.

More generally, quasars with Ca II troughs (and thus H I ionization fronts) that are detached in velocity enable a test to be made of the Murray et al. (1995) analytic disk wind model prediction of a monotonically decreasing velocity with increasing radius along the line of sight. Because the lowest velocity absorption arises outside the front, no absorption from high-ionization gas (e.g., C IV or N V) should be present at the lowest velocities. (Undetached troughs are not useful for this test because if the streamlines produce gas with zero velocity along the line of sight at one radius, they could easily produce such gas at many different radii.) Unfortunately, this test cannot be made in SDSS J0300+0048 because Fe II absorption obliterates the spectrum. It might be possible with spectra covering C IV in Ca II LoBALs with narrower troughs, such as FIRST J104459.6+365605, whose Ca II absorption is found at the low-velocity end of its higher velocity outflow (White et al. 2000; de Kool et al. 2001). On the other hand, the velocity distributions are the *same* for Ca II, excited Fe II, and excited He I absorption (which traces high-ionization He II) in the other two known Ca II LoBALs: QSO J2359−1241 (Arav et al. 2001) and Mrk 231 (Smith et al. 1995; Rupke, Veilleux, & Sanders 2002).

In fact, wide ranges of ionization states at identical velocities are often seen in BAL outflows (e.g., Arav et al. 1999). If disk wind models are to explain all BAL quasars, therefore, such models must at least sometimes produce a nonmonotonic velocity-distance relation or density inhomogeneities of some sort (such as clouds).

The associated absorption line system in SDSS J0300+0048 (see the Appendix) exhibits partial covering and therefore is likely located near the central engine. Whether it is associated with the BAL outflow is unclear. Blending of the AAL with the BAL trough shows that the spatial regions covered by the BAL outflow can vary significantly over velocity differences of $\sim$1700 km s^{-1}. Variations in the Mg I/Ca II ratio with velocity are also seen in both the BAL and AAL systems; these appear more likely to be due to variations in metallicity or abundances than in the ionization parameter.

In conclusion, in H02 we stated that "targeted high resolution spectroscopy of Ca II in SDSS J0300+0048 ... might determine if the column densities as well as the outflow velocities are very large." We have shown herein that the BAL outflow column densities are among the largest yet measured in BAL outflows. Furthermore, the highly ionized gas columns are as yet largely unconstrained. *Chandra* and possibly *XMM-Newton* observations will be able to constrain the total BAL column density regardless of ionization state.

We thank F. Barrientos, C. Churchill, H. Dickel, I. Strateva, J. Veliz, and the referee. P. B. H. acknowledges financial support from Chilean grant FONDECYT/1010981 and from Fundación Andes. Funding for the creation and distribution of the SDSS Archive has been provided by the Alfred P. Sloan Foundation, the Participating Institutions, the National Aeronautics and Space Administration, the National Science Foundation, the U.S. Department of Energy, the Japanese Monbukagakusho, and the Max Planck Society. The SDSS Web site is http://www.sdss.org/. The SDSS is managed by the Astrophysical Research Consortium (ARC) for the Participating Institutions. The Participating Institutions are the University of Chicago, Fermilab, the Institute for Advanced Study, the Japan Participation Group, the Johns Hopkins University, Los Alamos National Laboratory, the Max Planck Institute for Astronomy (MPIA), the Max Planck Institute for Astrophysics (MPA), New Mexico State University, the University of Pittsburgh, Princeton University, the United States Naval Observatory, and the University of Washington. This research has made use of the Atomic Line List v2.04 at http://www.pa.uky.edu/~peter/atomic/.

APPENDIX

THE ASSOCIATED ABSORPTION

We are interested primarily in the broad Ca II absorption, but there is narrow associated Ca II λ3934 blended with the broad Ca II λ3969. To remove this absorption, we must model the associated system.

To determine the continuum around each absorption line from the associated absorber, we make the simplifying assumption that the associated absorption is *external* to the broad absorption line region, an assumption we reconsider at the end of this section. Under this assumption, the locally measured continuum around each line is a good estimate of the true continuum seen by the associated absorber. Because there is structure near the associated Mg II that appears to be due to additional weak Mg II emission or absorption, we construct a local continuum for the associated Mg II by fitting a single polynomial continuum, offset only by a small flux difference, around both transitions in velocity space.

Figure 8 shows that the associated system is seen in Ca II, Mg II, Mg I, Fe II λ2600, and Fe II λ2382 (and Fe II λ2374, which is not plotted), but not in Fe II λ2586 (all these Fe II lines are from the lowest—i.e., unexcited—fine-structure level in the ground term of Fe II). We will return to this point at the end of this section. Ca II λ3969 and Mg I absorption are both weaker than Fe II λ2600 absorption, but their profiles are broadly consistent with the Fe II λ2600 absorption profile seen at lower optical depths. Because both ions exist only in gas with a low ionization parameter, they should show the same covering factors if they are saturated. We

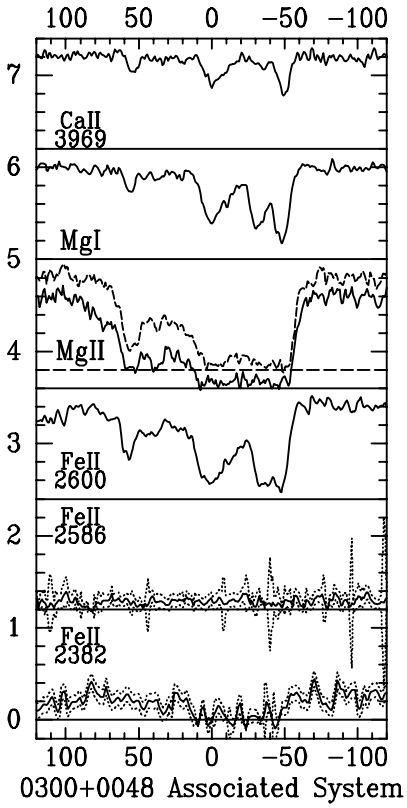

FIG. 8.—Transitions in the associated absorption system in SDSS J0300+0048. The vertical scale is the normalized flux density F_λ and the horizontal scale is the velocity in km s^{-1} (positive values for outflow). Each transition shown has been offset from the next by 1.2 normalized flux units in the vertical direction. Both lines of the Mg II doublet are plotted; the λ2803 line is plotted as a dotted line offset by +0.2 flux units. For two of the Fe II transitions, dotted lines are plotted to show the $\pm 1\ \sigma$ uncertainty ranges.

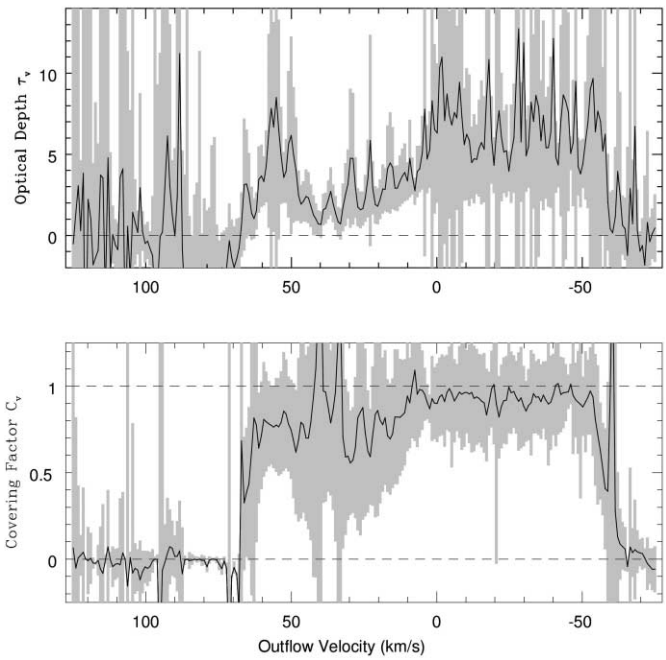

FIG. 9.—The thick black line gives the optical depth (*top*) and covering factor for associated Mg II as a function of velocity. The gray areas show the $\pm 1\ \sigma$ uncertainty ranges. The dashed lines delimit the ranges of physically valid solutions; namely, $\tau_v > 0$ and $0 \leq C_v \leq 1$.

conclude that the Ca II and Mg I absorption lines are unsaturated, with different τ_v. Overall, the associated absorption appears to have a higher Mg I/Ca II ratio than the broad absorption does (§ 4.3.1). Also, within the associated absorption itself, the subsystem at -32 km s^{-1} has a noticeably higher Mg I/Ca II ratio. This fact suggests the existence of inhomogeneities in the ionization, metallicity, or relative abundances as a function of velocity in the associated absorber (Churchill et al. 2003, and references therein).

We can use the unsaturated associated Ca II λ3969 absorption to model the optical depth in associated Ca II λ3934, but the Mg II absorption indicates that the associated absorber exhibits partial covering of the continuum source. Even though Mg II can occur in somewhat higher ionization gas than Ca II can, we can do no better than to assume that the associated Ca II has the same partial covering with velocity as Mg II.

The results of using equations (3) and (4) to compute C_v and τ_v for Mg II are shown in Figure 9. The absorber has $\tau_v \geq 1$ at almost every velocity. The observations are not quite consistent with $C_v = 1$ at all velocities: C_v appears lower at $v > 10$ km s^{-1} than at $v < 10$ km s^{-1}. Because the relative C_v of Ca II and Mg II are somewhat uncertain and the observed variations in C_v are consistent with the random noise, we will approximate C_v as a step function. From -54 to 10.5 km s^{-1} we find an average partial covering of $C = 0.93 \pm 0.04$ (with $\tau_{\rm Mg\,II} \simeq 7$). From 10.5 to 64 km s^{-1} we find an average partial covering of $C = 0.76 \pm 0.09$ (with $\tau_{\rm Mg\,II} \simeq 3$). There is additional absorption from 64 to about 93 km s^{-1} for which the (C, τ) fit breaks down because the 2796 Å absorption is less than half the strength of the 2803 Å absorption. It is likely that our continuum fit is in error at these velocities in one or both of the Mg II lines.

We now apply these two covering factors to the associated Ca II λ3969 absorption to predict the optical depth of the associated Ca II λ3934 absorption. If the associated absorption is external to the broad absorption, then—independent of any assumption about the true continuum incident on the broad absorption line region—the flux corrected for the associated Ca II λ3934 absorption F is related to the observed flux O by

$$O = F \times [1 - C \times (1 - e^{-R\tau})]\,, \qquad \text{(A1)}$$

where τ is the optical depth in Ca II λ3969 and all quantities except R are functions of velocity. We can recover F because we know O and R and have estimates for C and τ_{3969}. Figure 10 shows the spectral region around associated Ca II λ3934 before (*solid line*) and after (*dashed line*) this correction. The corrected spectrum appears reasonable everywhere except for a narrow spike near -53 km s^{-1}, which is interpolated over for our analysis.

A1. ASSOCIATED OR BROAD ABSORPTION: WHICH COMES FIRST?

Because the associated Ca II λ3934 spans such a narrow velocity range, our correction for it is not critical to the subsequent analysis of the BAL trough. Nonetheless, before proceeding it is worth considering further our assumption that the associated absorption arises outside the broad

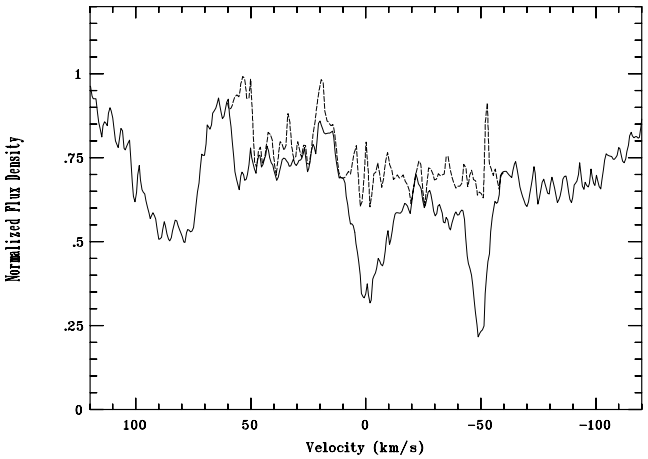

FIG. 10.—Region of the Ca II λ3969 BAL trough around the wavelength of associated Ca II λ3934 absorption. The solid line shows the observed, normalized spectrum, and the dashed line the spectrum with the associated Ca II λ3934 removed using the Ca II λ3969 profile and estimates for the optical depth and covering factor; see the Appendix. The corrected spectrum appears reasonable everywhere except for a narrow spike near -53 km s^{-1}.

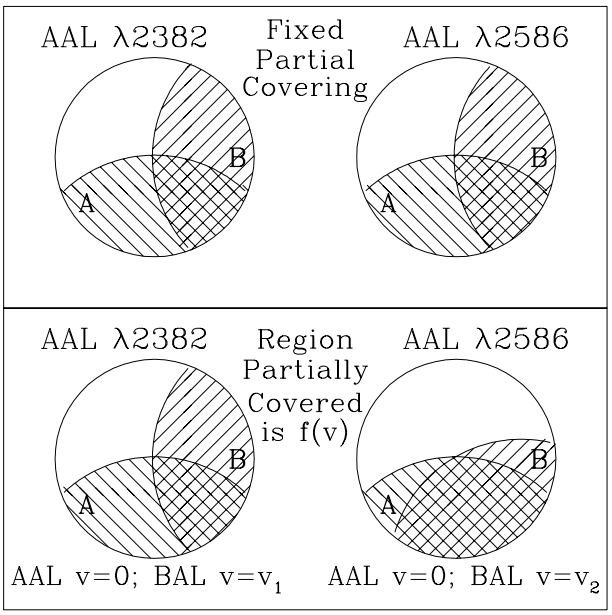

FIG. 11.—Schematic model of a quasar (*circle*) and absorption with partial covering. The lines slanting down and to the right show the source region covered by the narrow, associated, ground-state Fe II absorption (A), while the lines slanting up and to the right show the source region covered by the broad, excited Fe II absorption (B). The partial covering is shown at the redshifted wavelength of the associated Fe II λ2382 absorption on the left and at the redshifted wavelength of the associated Fe II λ2586 absorption on the right. As discussed in the text, the spatially fixed partial covering shown in the top panel cannot explain our observations. Instead, our data indicate that the broad absorption trough covers *different* regions of the quasar as a function of velocity, as shown in the bottom panel.

absorption line region. The probable partial covering of the associated absorber immediately calls into question this assumption, because partial covering is seen almost exclusively in gas linked with the central engines of AGN. However, while we cannot rule out a close connection between the associated and broad absorbers, we now show that neither can we rule out that the associated absorption arises near the nucleus but external to the broad absorption region.

The key insight comes from considering the associated absorption in Fe II $\lambda\lambda$2374, 2382 and Fe II $\lambda\lambda$2586, 2600—lines that all arise from the lowest fine-structure level in the ground term of Fe II. Between the redshifted wavelengths of the associated Fe II λ2600 and Fe II λ2586, the Fe II UV1 BAL (absorption from ground and excited states) removes most of the continuum, but not quite all (Fig. 1). If the associated absorption arises far out in the quasar host galaxy, we might expect to see Fe II λ2586 absorb $\sim$93% of the remaining continuum, just as Fe II λ2600 does. The normalized flux and ± 1 σ uncertainties in this spectral region are shown in the second panel from the bottom of Figure 8. Although the noise is large, there is no evidence for the expected absorption even when the spectrum is binned. However, there is clear evidence for Fe II λ2382 absorption (Figure 8, *bottom panel*). This spectral region is equally noisy, but in this case the absorption *is* consistent with being 93% of the surrounding continuum.[20] The same is true for Fe II λ2374, while the Fe II λ2344 region is too noisy for analysis.

The apparent lack of Fe II λ2586 absorption rules out the simple picture of a BAL trough and an associated absorption line system (AAL) that each absorb spatially fixed regions of quasar emission, shown schematically in the top panel of Figure 11. This conclusion applies even if the BAL or AAL regions are not well characterized by a single C and τ (de Kool et al. 2002b). To explain our observations requires some variation with velocity in the quasar emission region covered by the BAL trough. The bottom panel of Figure 11 is a sketch of this spatially distinct, velocity-dependent partial covering.

The reason the BAL region can partially cover spatially distinct emission regions at the wavelengths of the two associated Fe II transitions is that the broad Fe II absorption includes absorption from excited fine-structure levels, while the narrow Fe II absorption arises from only the ground level. At the zero-velocity wavelength of associated Fe II λ2382, the broad Fe II absorption can be approximated as having some velocity v_1. Because it consists of absorption in different Fe II multiplet UV2 transitions (both ground and excited) at different velocities, $v_1 = (1/N)\sum_i^N w_i v_i$, where w_i is the relative strength of line i at velocity v_i. Similarly, at the zero-velocity wavelength of associated Fe II λ2586, the broad Fe II absorption will consist of ground and excited Fe II multiplet UV1 transitions and can be approximated as having velocity $v_2 = (1/M)\sum_j^M w_j v_j$. The velocities v_1 and v_2 will be similar *but not identical*. Therefore, the covering factors can differ as well, both numerically $[C(v_1) \neq C(v_2)]$ and in the spatial regions covered. In SDSS J0300+0048, those different covering factors as a function of velocity allow the associated and broad Fe II absorbers to overlap the same spatial region at the wavelength of associated Fe II λ2586 but not at the wavelength of associated Fe II λ2382. This wavelength difference translates to a velocity difference $v_1 - v_2 \sim 1700$ km s^{-1} over which there must be considerable variation in the regions

[20] The local continuum used to normalize the Fe II λ2586 region in Fig. 8 is identical to that used for Fe II λ2600: it is flat in F_λ at the level of the spectrum just longward of Fe II λ2600. This same continuum was used to normalize the Fe II λ2382 region, for lack of a better assumption. However, the normalization does not affect the interpretation of why associated absorption from Fe II λ2586 was not detected.

being partially covered. Similar effects have been seen before in FBQS 1408+3054 (§ 6.1.2 of H02) and NGC 3783 (Gabel et al. 2003).

We cannot prove that the associated absorber is external to the BAL region, but we have shown that such a geometry, coupled with the spatially distinct, velocity-dependent partial covering that must be present, can explain our observations. We therefore used this "external" assumption to remove the associated Ca II absorption from the broad Ca II trough.

REFERENCES

Arav, N., Brotherton, M. S., Becker, R. H., Gregg, M. D., White, R. L., Price, T., & Hack, W. 2001, ApJ, 546, 140
Arav, N., Korista, K. T., de Kool, M., Junkkarinen, V. T., & Begelman, M. C. 1999, ApJ, 516, 27
Arav, N., & Li, Z. 1994, ApJ, 427, 700
Baldwin, J. A., Hamann, F., Korista, K. T., Ferland, G. J., Dietrich, M., & Warner, C. 2003, ApJ, 583, 649
Becker, R. H., White, R. L., Gregg, M. D., Brotherton, M. S., Laurent-Muehleisen, S. A., & Arav, N. 2000, ApJ, 538, 72
Blanton, M. R., Lin, H., Lupton, R. H., Maley, F. M., Miller, F., Young, R., Zehavi, I., & Loveday, J. 2003, AJ, 125, 2276
Boroson, T. A., & Green, R. F. 1992, ApJS, 80, 109
Branch, D., Leighly, K. M., Thomas, R. C., & Baron, E. 2002, ApJ, 578, L37
Churchill, C. W., Mellon, R. R., Charlton, J. C., & Vogt, S. S. 2003, ApJ, in press
Davidson, K., & Netzer, H. 1979, Rev. Mod. Phys., 51, 715
de Kool, M., Arav, N., Becker, R. H., Gregg, M. D., White, R. L., Laurent-Muehleisen, S. A., Price, T., & Korista, K. T. 2001, ApJ, 548, 609
de Kool, M., Becker, R. H., Arav, N., Gregg, M. D., & White, R. L. 2002a, ApJ, 570, 514
de Kool, M., Korista, K. T., & Arav, N. 2002b, ApJ, 580, 54
Everett, J. E. 2003, ApJ, submitted (astro-ph/0212421)
Fan, X., et al. 1999, ApJ, 526, L57
Ferland, G. J., & Persson, S. E. 1989, ApJ, 347, 656
Fukugita, M., Ichikawa, T., Gunn, J. E., Doi, M., Shimasaku, K., & Schneider, D. P. 1996, AJ, 111, 1748
Gabel, J. R., et al. 2003, ApJ, 583, 178
Ganguly, R., Eracleous, M., Charlton, J. C., & Churchill, C. W. 1999, AJ, 117, 2594
Graham, M. J., Clowes, R. G., & Campusano, L. E. 1996, MNRAS, 279, 1349
Gunn, J. E., et al. 1998, AJ, 116, 3040
Hall, P. B., et al. 2002, ApJS, 141, 267 (H02)
Hall, P. B., & Hutsemékers, D. 2003, in ASP Conf. Ser. 290, Active Galactic Nuclei: From Central Engine to Host Galaxy, ed. S. Collin, F. Combes, & I. Shlosman (San Francisco: ASP), in press
Hamann, F., Barlow, T. A., Chaffee, F. C., Foltz, C. B., & Weymann, R. J. 2001, ApJ, 550, 142
Hamann, F., Barlow, T. A., Junkkarinen, V., & Burbidge, E. M. 1997, ApJ, 478, 80
Hogg, D. W., Finkbeiner, D. P., Schlegel, D. J., & Gunn, J. E. 2001, AJ, 122, 2129
Horne, K. 1986, PASP, 98, 609
Joly, M. 1989, A&A, 208, 47
Junkkarinen, V. T., Burbidge, E. M., & Smith, H. E. 1983, ApJ, 265, 51
Kwan, J., Cheng, F., Fang, L., Zheng, W., & Ge, J. 1995, ApJ, 440, 628
Lupton, R. H., Gunn, J. E., & Szalay, A. S. 1999, AJ, 118, 1406
Murray, N., Chiang, J., Grossman, S. A., & Voit, G. M. 1995, ApJ, 451, 498
Pier, J. R., Munn, J. A., Hindsley, R. B., Hennessy, G. S., Kent, S. M., Lupton, R. H., & Ivezic, Z. 2003, AJ, 125, 1559
Proga, D. 2003, ApJ, 585, 406
Proga, D., Stone, J. M., & Kallman, T. R. 2000, ApJ, 543, 686
Richards, G. T., et al. 2002, AJ, 123, 2945
Rupke, D. S., Veilleux, S., & Sanders, D. B. 2002, ApJ, 570, 588
Savage, B. D., & Sembach, K. R. 1991, ApJ, 379, 245
Shakura, N. I., & Sunyaev, R. A. 1973, A&A, 24, 337
Sigut, T. A. A., & Pradhan, A. K. 2003, ApJS, 145, 15
Smith, J. A., et al. 2002, AJ, 123, 2121
Smith, P. S., Schmidt, G. D., Allen, R. G., & Angel, J. R. P. 1995, ApJ, 444, 146
Srianand, R., & Shankaranarayanan, S. 1999, ApJ, 518, 672
Stoughton, C., et al. 2002, AJ, 123, 485
Verner, E. M., Verner, D. A., Korista, K. T., Ferguson, J. W., Hamann, F., & Ferland, G. J. 1999, ApJS, 120, 101
Vestergaard, M., & Wilkes, B. J. 2001, ApJS, 134, 1
Voit, G. M., Weymann, R. J., & Korista, K. T. 1993, ApJ, 413, 95
Wampler, E. J., Chugai, N. N., & Petitjean, P. 1995, ApJ, 443, 586
Weymann, R. J., Morris, S. L., Foltz, C. B., & Hewett, P. C. 1991, ApJ, 373, 23
White, R. L., et al. 2000, ApJS, 126, 133
York, D. G., et al. 2000, AJ, 120, 1579